UNIVERSITY OF CALIFORNIA, SAN DIEGO

Dynamic Surface Topography Influences Cell Function

A thesis submitted in partial satisfaction of the requirements for the degree of Master of Science

in

Bioengineering

by

Jennifer Deng Kiang

Committee in charge:

Professor Adam J. Engler, Chair
Professor Shyni Varghese
Professor Juan Carlos del Alamo

2012

The Thesis of Jennifer Deng Kiang is approved and it is acceptable in quality and form for publication on microfilm and electronically:

_____

_____

_____

Chair

University of California, San Diego

2012

TABLE OF CONTENTS

NOMENCLATURE

MSC	mesenchymal stem cell
BMSC	bone marrow-derived mesenchymal stem cell
μm	micrometer
nm	nanometer
kPa	kilopascal
PA	polyacrylamide
mL	milliliter
mm	millimeter
cm	centimeter
OCT	optimal cutting temperature
dH_2O	distilled water
min	minutes
RPM	rotations per minute
sec	seconds
NaOH	sodium hydroxide
APS	ammonium persulfate
DCDMS	dimethyldichlorosilane
TEMED	tetramethylethylenediamine
UV	ultraviolet
HEPES	2-[4-(2-hydroxyethyl)piperazin-1-yl]ethanesulfonic acid
μg	microgram
PBS	phosphate buffered saline
NdFeB	neodymium
T	Tesla
AFM	atomic force microscope
mg	milligram
BSA	bovine serum albumin
hr	hour
nN	nano-Newton
DMEM	Dulbecco's Modified Eagle Medium
FBS	fetal bovine serum
mM	millimolar
LB	lysogeny broth
TXRD	Texas Red
ANCOVA	analysis of covariance
Hz	Hertz
SEM	standard error of the mean

LIST OF FIGURES

LIST OF TABLES

ACKNOWLEDGEMENTS

I would like to Professors Engler, Varghese, and del Alamo for their time and expertise in the preparation and presentation of my thesis. I would particularly like to thank my advisor, Dr. Engler, for his continual guidance and support in both my research and my development as a scientist and engineer. I would also like to acknowledge Dr. Sungho Jin at UCSD for his advice on microwire fabrication, and Dr. Nathan Sniadecki at the University of Washington for his general help and advice on the development of this project. Finally, I would like to thank the Engler lab for their advice and encouragement throughout the last two years. In particular, I would like to thank Somyot Chirasatitsin for help with the AFM, Ludovic Vincent for his knowledge on PA hydrogel polymerization and TFM, Yu Suk Choi for his help with cell culture, and Jessica Wen for always being a great resource to discuss problems and new ideas.

ABSTRACT OF THE THESIS

Dynamic Surface Topography Influences Cell Function

by

Jennifer Deng Kiang

Master of Science in Bioengineering

University of California, San Diego, 2012

Professor Adam J. Engler, Chair

Micro- and nano-scale changes in surface topography can modulate mesenchymal stem cell (MSC) differentiation; rough surfaces have been shown to induce osteogenesis to varying degrees depending on the scale and nature of the topographical features. However, in the *in vivo* environment, topography is constantly changing due to remodeling by cells within the niche. To better understand how mesenchymal stem cells respond to changes in topography over time, we developed a soft polyacrylamide hydrogel with magnetic nickel microwires randomly oriented in the surface of the material. Varying the magnetic field around the microwires can reversibly induce their alignment with the direction of the field, causing the smooth hydrogel surface to develop small wrinkles. By varying the density of wires in the hydrogel, surface roughness changes, ΔR_{RMS}, ranged from 0.09 μm (wire-free substrates) to 0.52 μm (maximum wire density) a custom displacement mapping software. Time-dependent topographical changes were achieved by oscillating the field around the microwires using step function or cyclic changes. Smooth muscle cells plated onto these substrates changed morphology by shrinking within minutes of inducing a step change in topography. However, on a longer time scale characterized by a

continual modulation of topography, cells show no appreciable response, likely due to their propensity to remodel over longer time scales. Being able to dynamically study how cells respond to changes in topography will improve our current understanding of topography-driven effects on cell behavior, and eventually, on stem cell differentiation.

Chapter I

INTRODUCTION

1.1. Factors Implicated in Mesenchymal Stem Cell Differentiation

Mesenchymal stem cells (MSCs) are a class of multipotent adult stem cells that can self-renew, and differentiate into mesodermal lineages in response to specific microenvironmental niches, which are comprised of various soluble and insoluble chemical, structural, and mechanical factors [1]. Being able to control lineage expression in these cells, particularly at a high efficiency, has significant clinical applications where MSCs could be used to provide growth factors for tissue repair, or they themselves could repair or regenerate tissue damaged by disease, injury, or age. However, these *in vivo* microenvironments are very complex, and thus far have proved very difficult to replicate *in vitro*, often resulting in significant heterogeneity in the differentiated cell population[2].

The mechanical and structural factors that contribute to differentiation cues for MSCs can be broadly broken down into components such as matrix stiffness, architecture, and other external forces[3], but this thesis concentrates on the role of topography, specifically how its modulation over time may affect cell behavior. Being able to dynamically study how cells respond to changes in topography will improve our current understanding of topography-driven effects on cytoskeletal assembly and remodeling, and eventually, on stem cell differentiation. This idea of topography, however, is also inherently coupled to substrate stiffness, as will be discussed. Prior to discussing the current work in this thesis, however, it is necessary to provide a concise review of the state of the field concerning the influence of topography on cell behavior.

1.2. Current Work in Micro- and Nano-topography to Influence Cell Behavior

While many studies have examined the role of topography in conjunction with chemical differentiation factors [4, 5], recent work has demonstrated that topography alone, in the absence of any chemical cues, can alter cell behavior. These topography-dependent characteristics include adhesion [6, 7], migration [8, 9], morphology [10], growth [11, 12], proliferation [13], and in particular, MSC differentiation[14].

The idea of topography in this application encompasses all aspects of surface shapes and features including the type, size, and organization of features. Surface chemistry (e.g. ligand type, patterning, spacing and density) is also often categorized into this field. While all of these characteristics are relevant to topography, it is an exceedingly broad categorization because of the widely heterogeneous effects that different types and scales of topography can have on cells. Additionally, even in the absence of any chemical factors, topography is also inherently coupled to other types of extracellular cues, namely, substrate stiffness. Thus the discussion here as well as the thesis question of dynamic topography will be limited to submicron roughness changes.

1.2.1. Types of Topographical Features

The first aspect of micro- and nano-topography to be discussed is the type of feature studied, which is closely tied to the fabrication technique, i.e. electrospinning, lithography and etching, and phase separation, among other methods. Electrospinning creates a fibrous mesh to which cells can adhere. The mesh is fabricated by applying a strong electric field to a droplet of (usually polymer) solution, which stretches it and causes it to solidify into micro- to nano-scale fibers. Electrospun nanofibers made of synthetic polymers have been shown to drive bone marrow-derived MSC's (BMSC's) to neuronal [4], epidermal [15], and chondrogenic [16] lineages depending on the growth factors added. Despite growth factor signaling, stem cell induction via electrospun fibers has varied widely with similar conditions, resulting in both

osteogenic and adipogenic lineages [17]. The use of silk nanofibers, however, has been shown to encourage osteogenesis. Electrospinning allows for fine control over the fiber diameter, and the mixture of polymers at the monomer, fiber, and scaffold levels. The biggest drawback of electrospun fiber networks is the lack of control over matrix porosity[18].

Lithography is a technique used to create micro- and nano-pillars and grooves, as opposed to a 3D fiber network. The lithographic process starts by selectively exposing parts of a light- or electron-sensitive material using a patterned mask, selectively removing the resist and leaving parts of the material susceptible to etching, resulting in features such as pillars and grooves. UV lithography is the most common technique used, and can develop features down to 1 μm [19, 20]. Electron beam lithography has also become popular to fabricate nanoscale features with lateral resolution of less than 10 nm [19]. It has recently been used to synthesize pits and islands, in addition to grooves and pillars [21]. While lithography can generate a variety of features in regard to both scale and geometry and can be scalable to fit the throughput required for an application, it is an expensive and time-consuming fabrication process. Lithography has been used in many instances to modulate BMSC differentiation. For example, a reverse casting of a PDMS mold with 13 μm grooves from a lithographically-patterned wafer was shown to upregulate neuronal markers in BMSC's [22]. 200 nm alumina and titania nanoparticles have also been shown to improve MSC cell adhesion and self-renewal [23, 24].

Polymer phase separation is another topography fabrication technique used to create micro- and nano-scale pits and islands in which microphase separation of dissimilar diblock copolymers, which may separate due to effects such as charge, phobicity/philicity, or solvent miscibility, create domains of dissimilar height. Typically it is difficult to control the order of these nanoscopic features, as phase separation is not patterned in any way, bus a recent study was able to create more controlled patterns by tethering phase-separating polymer blocks to yield

inverse micelles [25]. Polymer phase separation has been used to demonstrate modulation of functions such as cell adhesion, spreading, proliferation, and differentiation [26].

1.2.2. Topographical Feature Size

In its microenvironment, a cell will feel not only feel the geometry of the surfaces surrounding it, but the scale of those surfaces as well, e.g. porosity can dictate the effective dimensionality of a microenvironment. Individual cells interact with features ranging from microns (such as the organization of surrounding cells and matrix fibrils) to nanometers (such as ligand presentation). Thus, in addition changing feature type, various groups have looked at the effect of modulating the size of their surface features while maintaining a constant geometry.

One particular area of interest has been to better define the upper and lower limits of topography that a cell will respond to. However, there still appears to be disagreement as to its effects. Amongst varied feature types (e.g. pits, pillars), several reports indicate that cells appear to become smaller and rounded with less organized cytoskeletons when the feature size falls below 5 μm [19]. Other studies report that focal adhesion formation and cellular responses are impaired between the 50nm through the micron-level, but that stem cell adhesion and differentiation are improved on either a smaller or larger scale. These studies also looked at a variety of topographical features (e.g. pillars, islands, pits) [14].

Finally, the application of carbon nanotubes to the question of topographical effect has also yielded distinctive results. Oh, et al. found nanotubes with a 100nm diameter promoted osteogenic differentiation of MSC's significantly more than those cultured on nanotubes with <50nm diameter [27].

There is still considerable discrepancy in the literature regarding the effect of topography size on cell behavior. Many of the reviews in this area attempt to draw conclusions from studies that use widely varying types of topographical features that have been fabricated using different

methods, and have different inherent stiffnesses. It is likely that the inconsistent conclusions are a result of these other factors; i.e. it seems premature to draw conclusions without more control of the variables involved.

1.2.3. Spatial Organization of Topographical Features

Many of these topographical patterns, notably grooves, islands, and pits fabricated by lithography, have a repeating order, or pattern. This also has a significant effect on how cells respond. In the case of groove-like structures, while the degree of response was dependent on the cell type and groove characteristics, cells generally aligned and elongated in the direction of the groove. This characteristic has proved valuable as a means of contact guidance for neuronal-type cells [22]. It has also been shown that no cell type thus far (with the exception of red blood cells) will respond to features placed more than 20 μm apart [19]. In regard to pits, it has been found that MSC's respond much more strongly down an osteogenic lineage when confronted with an array of pits with controlled disorder, in comparison to a perfectly ordered pattern [21]. These examples demonstrate that the disparity between highly ordered and disordered patterns can result in significant differences in the morphology and differentiation of cells.

1.3 Effect of Substrate Stiffness on Stem Cell Differentiation

Independent of topography type, size, organization, or frequency, all topographical features must be made in some material, and that material has an inherent Young's modulus, *E*, or "stiffness", which can be measured from the stress-strain relationship when a material is undergoing tensile loading. Therefore, it is also important to mention substrate stiffness as a consideration for cell behavior, especially given its previously documented influence on MSC differentiation. It has been shown for a range of physiological stiffnesses (1, 11, and 34 kPa), that in the absence of any chemical factors, MSC's can be induced towards neuronal, myogenic, and osteogenic lineages by substrate stiffness alone [28]. All topography studies thus far have been

performed on relatively stiff substrates, for example, polydimethylsiloxane (PDMS), poly(methylmethacrylate) (PMMA), polystyrene (PS), silicon, carbon nanotubes, and others [19]. As such, all effects on topography have been performed while coupled to a stiff substrate. This is an obvious limitation to the work done so far to elucidate the role of topography on stem cell differentiation. What would be the effect of topographical features on a soft substrate? This project proposes a platform that would allow for a modulation in substrate stiffness, as well as modulation of topography in both space and time.

1.4. Thesis Organization

This thesis provides a summary of a novel cell culture substrate platform that relies on the magnetic actuation of micron-scale magnetic particles embedded in a PA hydrogel to reversibly induce a random surface topography in a soft material to which cells can respond. Varying the magnetic field around the microwires can reversibly induce their alignment with the direction of the field, causing the smooth hydrogel surface to develop small wrinkles. Details of the fabrication of the microwires and the hydrogel are described in Chapter II. Chapter III discusses the response of cells on this substrate in two cases: the first being a step function change in topography from smooth to rough, and the second being a prolonged oscillation between the rough and smooth states. A summary of this project and the implications of its results are laid out in Chapter IV.

Chapter II

Material Synthesis and Characterization

2.1. Material Synthesis

This topographically dynamic cell culture substrate is composed of a soft polyacrylamide hydrogel with magnetic microwires embedded near the surface to induce reversible deformations, or "wrinkles" which cells can then respond to. This chapter discusses the protocol used to synthesize this hydrogel platform, as well as its subsequent material characterization.

2.1.1 Synthesis of a Two-Layer Polyacrylamide Hydrogel System

Polyacrylamide hydrogels are a common biomaterial used for cell culture composed of acrylamide and bis-acrylamide monomers that are connected by free radical polymerization. The side chains of the bis-acrylamide monomers are used to cross-link the acrylamide chains into a mesh (Figure 2.1). A major benefit to the polyacrylamide hydrogel system is that surface chemistry can be kept constant while changing its mechanical properties [29]. The concentration of acrylamide and bis-acrylamide can be modulated to yield hydrogels with varying Young's moduli while keeping the surface chemistry constant [29]. For my application, a PA hydrogel with a Young's modulus of 1 kPa was used; the acrylamide and bis-acrylamide contents are as follows:

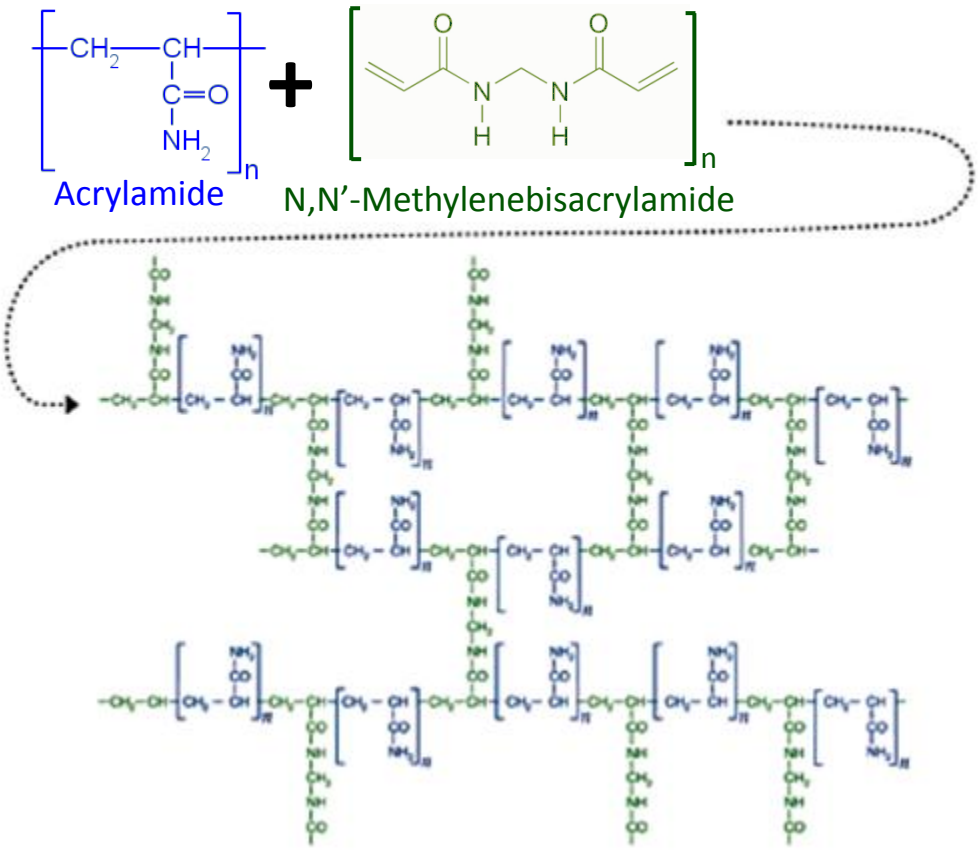

Figure 2.1. Schematic of polyacrylamide hydrogel assembly by free radical polymerization.

Table 2.1. Adapted from [29]. The relative concentrations of acrylamide and bis-acrylamide and their expected modulus of elasticity. The volumes in the last three columns make a total volume of 10 mL of hydrogel solution. APS and TEMED are added at volumes of 1% and 0.1%, respectively.

Hydrogel Stiffness (kPa)	Acrylamide %	Bis-Acrylamide %	Acrylamide from 40% stock (mL)	Bis-acrylamide from 2% stock (mL)	Water (mL)
1.00 ± 0.31	5	0.03	1.25	0.15	8.6

Relatively soft hydrogels were used in order to maximize the deformation induced by the magnetic torqueing of the microwires. These PA hydrogels were polymerized onto 25 mm glass coverslips that had been activated by amino-silanation to covalently bind the hydrogel to the surface of the coverslip. As this could potentially be developed to drive mesenchymal stem cell differentiation, it should be noted that these stiffnesses on static PA hydrogels correspond to differentiation to a neuronal-like cell lineage [28].

For this substrate, a dual-layer hydrogel system using a two-step polymerization process was adopted. It was necessary to confine the magnetic particles to the surface of the hydrogel so that they would provide a maximal torque on the surface. This was achieved by first polymerizing a thick layer of PA, adding a small volume of wires suspended in solution, then polymerizing a thin layer of PA on top of that. This system allows for the wires to remain confined to the top surface of the hydrogel where they can transduce the maximal force to deforming the hydrogel surface, while eliminating any effect of the high elastic modulus of the glass coverslip underneath.

2.1.2. Magnetic Particle Selection and Fabrication

Three types of magnetic nickel particles were polymerized into the top surface of the hydrogel. First, nickel nanowires (courtesy of Dr. Nathan Sniadecki at the University of Washington) (20 μm in length by 300 nm diameter), synthesized by electrolysis of a nickel

solution through an Anodisc filter were used [30]. With the strongest magnetic field available (see section 2.2.1), these nanowires proved to be too small, creating too little force to deform the hydrogel. As shown in Figure 2.2, only the aligned bundles of wires that sometimes associated (usually ~1 μm in diameter) had enough torque to visibly deform the gel; the individual nanowires did not. The same conclusions resulted from tests with spherical nickel microbeads as well (1-4 μm diameter, Thermo Scientific #21353), where they did not generate enough force from the magnetic field to cause any topographical changes in the hydrogel. Based on the previous observations with aggregate wire bundles of this size, the magnetic particle size required to produce a response was at least 1 μm in diameter and 20 μm in length. Unfortunately, no such wires are commercially available, so a microwire fabrication procedure to make wires to these specifications was developed.

2.1.3. Microwire Fabrication

To fabricate microwires to these specifications, a 50 cm segment of 0.025 mm diameter nickel wire (#40672, Alfa Aesar) was used, cut it into ~1 cm lengths, and etched in a dilute acid solution of one part nitric acid and one part dH_2O (prepared immediately before use) for 20 min. This yielded a wire diameter of approximately 5 μm. The etching was terminated by diluting the acid solution out with water and embedding the resultant wires in Optimal Cutting Temperature (OCT) compound. The wires were all aligned to the same orientation by application of magnetic field. Once the wires were frozen in solid state OCT, they were cryosectioned into 20 μm lengths by cutting sections perpendicular to the wire axis.

To purify the wires, the OCT sections were diluted with 10 mL of dH_2O, mixed well, and centrifuged for 5 min at 2000 RPM to sediment the OCT and any remaining debris. The wires were then precipitated with a magnet, and the remaining solution discarded. Another 10 mL of dH_2O were added, the solution and wires mixed well, then spun down again for another 5 min at

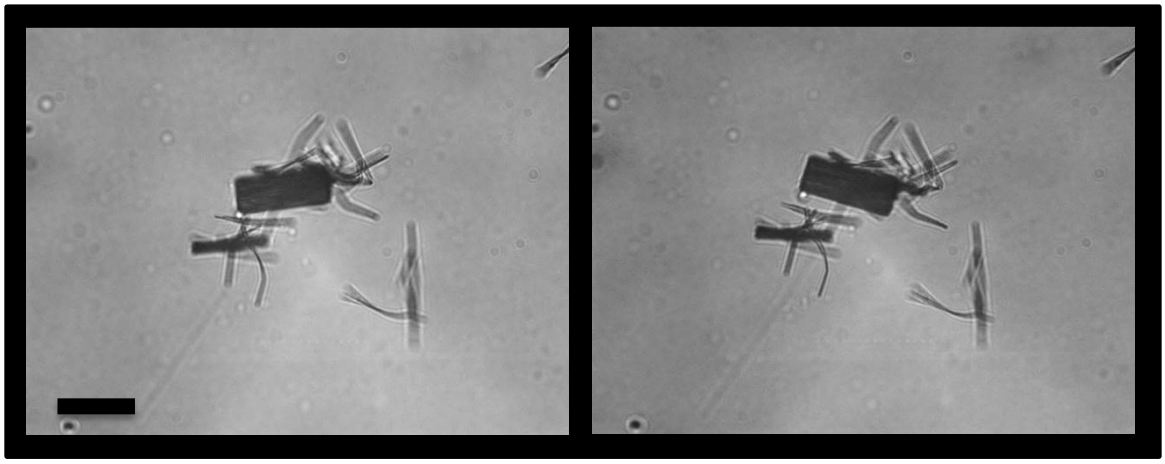

Figure 2.2. Nickel nanowires polymerized in a 1 kPa two-layer PA hydrogel in a neutral state (left) and in the presence of a magnetic field (right). Scale bar = 20 μm.

2000 RPM. Again, the wires were precipitated and the residual solution discarded. The wires were then suspended in dH_2O. The wires were vortexed for 30 sec, sonicated for 10 min, autoclaved, and vortexed and sonicated again immediately prior to every use.

2.1.4. Fabrication of Microwire-Embedded PA Hydrogels

The microwire-embedded hydrogels were fabricated by the protocol briefly described in section 2.1.1. Amino-activated glass coverslips were made based on previous methods [29]. In summary, aminosilanation was achieved by drying NaOH uniformly onto the coverslip, adding APES, washing with dH_2O, then incubating in gluteraldehyde. Coverslips were then dried from excess gluteraldehyde and ready for use. Hydrogels were made on DCDMS-coated slides to make them hydrophobic so that the hydrogels would only adhere to the amino-activated coverslips, and not the opposing slide. To make the two-layer hydrogels, the acrylamide/bis-acrylamide solution could be made ahead of time and stored; the APS and TEMED were added immediately prior to polymerization. After adding the initiator, a 20 μL drop of wire solution was added to the hydrophobic slide, then a coverslip with its activated side down was carefully placed on top of it. Once the first hydrogel was polymerized (~20 min), the coverslip with attached hydrogel was separated from the slide, and a 20 μL drop of wire solution was dropped onto the hydrogel and carefully spread with the side of a 20 μL pipette tip. Any residual water sitting on the hydrogel was pipetted off, and another 8 μL of hydrogel solution was dropped onto the slide. The coverslip was inverted (gel side down) to cover it. Once the second layer had polymerized, the hydrogel was rinsed in dH_2O and allowed to hydrate for at least 30 min before being coated with protein to promote cell adhesion. The coverslip was immersed in Sulfo-SAMPAH, a heterobifunctional protein cross-linker, and activated by UV light (305 nm wavelength) for 10 min. The hydrogel was then washed three times in HEPES buffer under

sterile conditions and incubated with 10 μg/mL of human fibronectin at 37°C for at least two hours. The hydrogels were then rinsed in PBS and ready for use.

2.2. Material Characterization

Two-layer PA hydrogels embedded with magnetic microwires deviate from previously characterized PA hydrogels due to their multi-step polymerization and inclusion of wires[29]; therefore, surface properties and hydrogel mechanics were measured. Since the hydrogel is polymerized in two steps, the identical layers may mix, re-polymerizing and interacting with each other to change overall hydrogel stiffness. Introduction of nickel microwires into the substrate may also change local stiffness. Given the repeated cycles of an oscillating magnetic field, it was also important to test for viscoelastic creep to ensure the integrity of the topographical features over time.

2.2.1 Magnetic Field-Induced Change in Topography

The next step after developing the substrate was to confirm and quantify the changes in topography between rough and smooth states. Confocal microscopy would not resolve the topographical features because of the size of the features, and the lack of z-resolution. Therefore, traction force microscopy was used to visualize the surface topography. The magnetic field used in this experiment and the subsequent cell morphology experiments utilized two aligned NdFeB block magnets, each exerting a magnetic field of 0.31 T [30] with a small separation in the middle (Figure 2.3). Therefore, the field was primarily perpendicular to the plane of the hydrogel. It should be noted though, that this cannot be used as a predictor of the features that the wires will create because the wires are oriented randomly.

Using an image analysis software developed by Dr. Juan Carlos del Alamo, traction force microscopy was performed on the hydrogels to detect displacements and traction forces in 3D. It was originally developed to look at traction forces that single cells will exert on a deformable

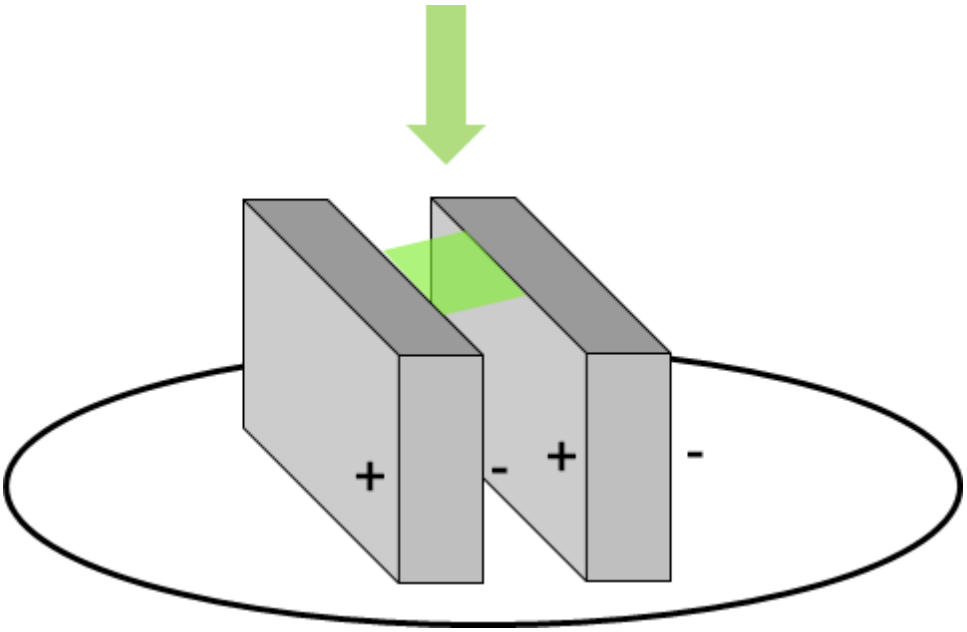

Figure 2.3. Schematic of magnet orientation used to acquire confocal stacks for traction force microscopy.

hydrogel, but it was used in this project to visualize the features created by the microwires deforming the hydrogel. Since the software relies on a fluorescent particle tracking algorithm, 0.1 μm fluorescent microspheres (Invitrogen, #F8803) were added to the hydrogel during the polymerization step at a concentration of 30 μL per mL of PA solution. The beads were added to the unpolymerized solution, vortexed for 30 sec, and sonicated for 10 min to ensure even distribution. APS and TEMED were added to initiate polymerization. For the purposes of the experiment detailed here, the only relevant deformation was in the surface of the hydrogel, so fluorescent beads were only added to the 8 μL upper hydrogel layer. Two sets of confocal z-stack images were taken through the top layer of the hydrogel (usually about 10-15 μm thick with one z-stack every 0.4 μm) to capture bead positions in the undeformed state as well as in the magnetic field-induced "rough" state. The traction force software was then able to track groups of particles to compute the displacements of the hydrogel in x-, y-, and z-dimensions (Figure 2.4A, B).

Samples with varying wire concentrations were analyzed, and a relatively strong positive correlation was found between wire density (as measured by the ratio of wire area to total view area), and surface roughness (Figure 2.4C).

2.2.2 Comparison of Topographical and Lateral Displacements

PA hydrogels are almost entirely water, and thus experimentally-determined Poisson's ratios range from 0.33-0.45 [31]. This translates into the fact that being an elastic solid, any perturbation caused by a wire in the z-direction will be equally compensated in the x- and y-directions. Because this project focuses on the effect of topography and not strain, on cell morphology, it was important to verify that majority of the displacements within the hydrogel occurred in the z-direction. This was analyzed by looking at all of the images used to characterize the surface roughness, and additionally looking at the x- and y- displacements at each point, in addition to the z-displacements. For each frame of view, the x- and y-displacements

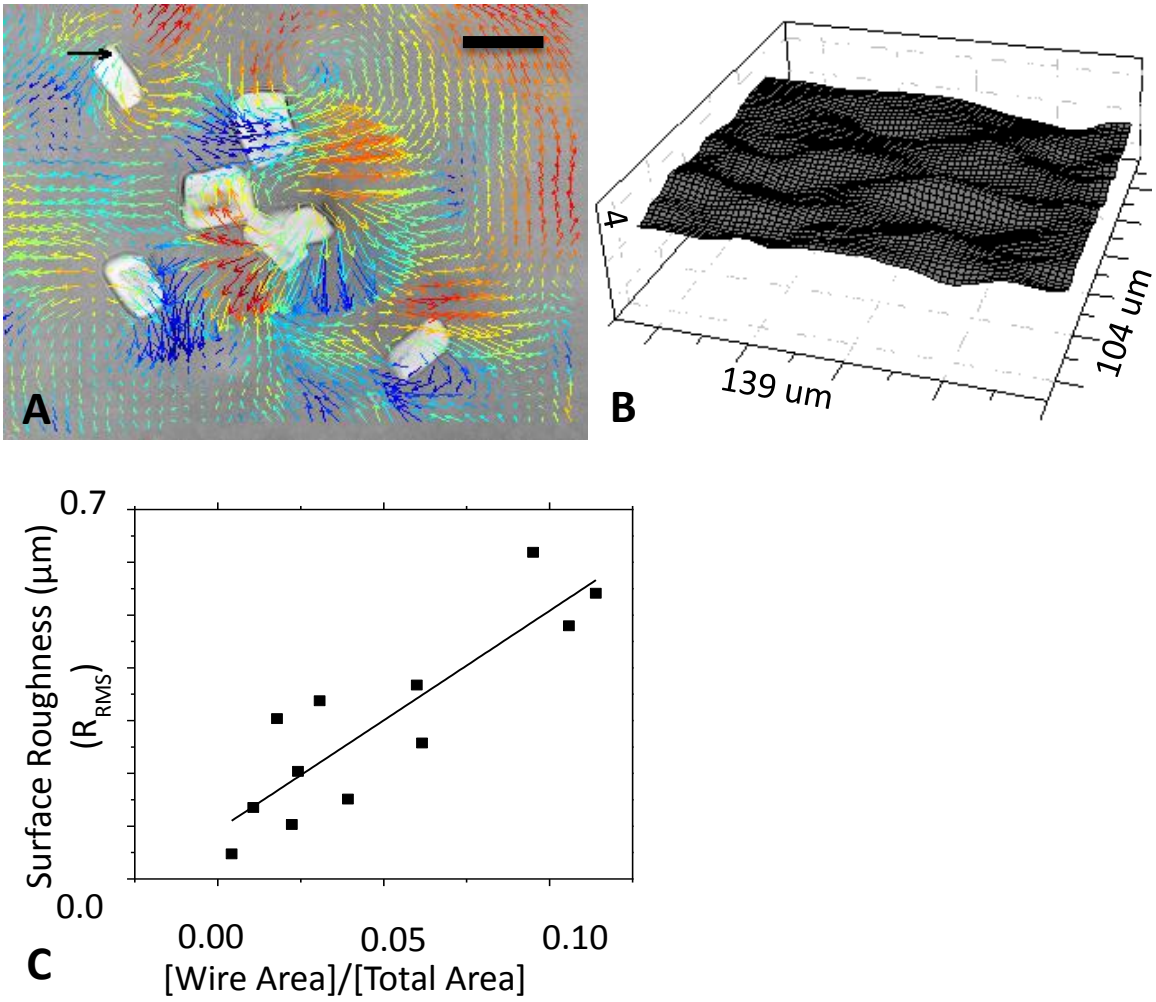

Figure 2.4. Microwire-embedded matrix characterization. **(A)** Displacement field induced by microwires in a 0.31 T magnetic field from traction force microscopy (TFM) analysis. Scale bar = 20 μm **(B)** Topographical map of surface feature changes, features are on the order of 0.5-1.0μm. **(C)** TFM analysis shows a positive correlation between the root-mean-square surface surface roughness (R_{RMS}) and wire density; y=4.1542x + 0.0928, R^2=0.744.

at each point were compared to the z-displacement to create a map where the x- and y-displacements exceeded the z-displacements and vice versa (Figure 2.5A). Global displacement ratios, regardless of substrate roughness, were also expressed as the ratio of z-displacements averaged over the entire image, to the averaged x- and y-displacements to give a general 'displacement ratio'. A value greater than 1 would imply a greater deformation in the z-, than in the x- or y-directions. Figure 2.5B shows that while there was considerable variability between the samples, in general z-displacements exceeded x- or y-displacements.

2.2.3 Atomic Force Microscopy

In addition to topography, i.e. ΔR_{RMS}, the static hydrogel properties, including elastic modulus and topography, also required characterization. The atomic force microscope (AFM) is essentially a very sensitive cantilever that can detect micro- to nano-scale changes in topography and modulus. Figure 2.6 illustrates the mechanics of the AFM. A cantilever tip is attached to the cantilever point, and a laser is directed onto the cantilever tip to produce a deflection beam to some point in its resting state. The cantilever is attached to a piezo-electric motor to ensure fine z-direction control. As the tip approaches and touches the surface, there is no change in deflection, but once it contacts the material, increasing indentation results in increasing force imparted on the material from the cantilever. Based on the change in deflection in relation to the distance that the cantilever moves in the z-direction, the modulus and topography of the sample can be calculated[32].

For this experiment, a gold-plated pyramidal cantilever tip was used because of the fine spatial detail that it can resolve. Also, the hydrogel samples were coated in 1 mg/mL bovine serum albumin (BSA) for 12-24 hr before imaging to counter hydrophobic effects. The AFM tip and sample are both very prone to interactions, meaning that when the tip contacts the hydrogel surface, it is resistant to release. This "stickiness" can impede the collection of measurements.

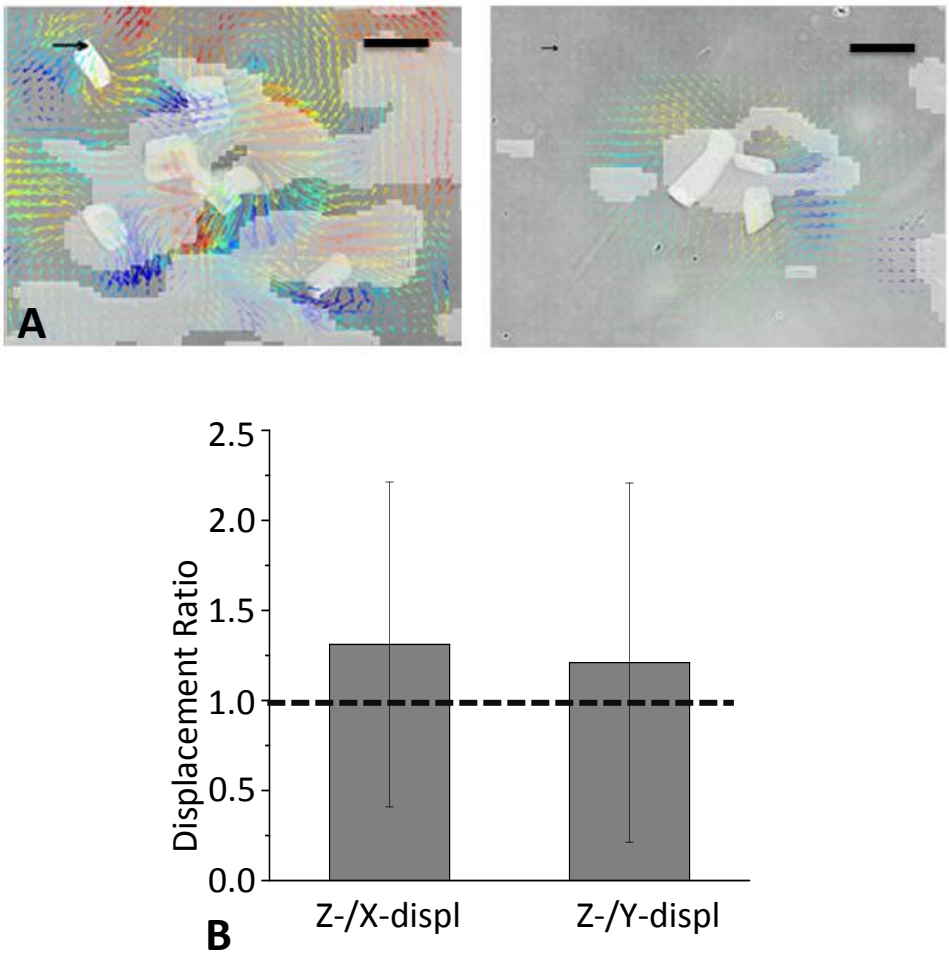

Figure 2.5. (A) Brightfield displacement map (with x- and y-displacements denoted by the direction and magnitude of the arrows, and z-displacements denoted by color) overlaid with shaded maps of displacement comparison. The white areas indicate regions where the x- and y-displacements exceed the z-displacements. **(B)** Overall, the z-displacements exceed both the x- and y-displacements (i.e. the displacement ratio is greater than 1).

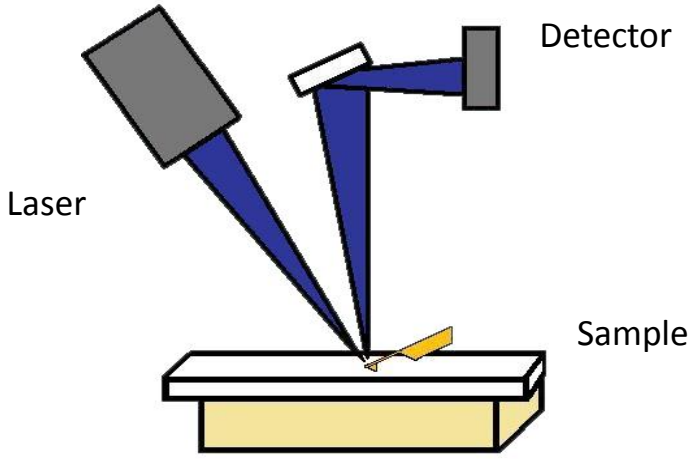

Figure 2.6. Schematic of AFM mechanism. A laser is directed at the pyramidal cantilever tip, which then deflects light to a point on the detector. When the cantilever tip indents into the sample, it bends slightly and changes the position of the deflection beam.

The BSA provides an inert coating to minimize any interactions between the tip and hydrogel surface. Because this substrate is very soft and "sticky", a low trigger force (3 nN) and high force distance (7-8 μm) were used. A low trigger force signals the tip to release without indenting very deeply into the sample, and a high force distance allows the tip to move 7-8 μm in the z-direction, to minimize the likelihood that the tip will remain bonded to the surface of the hydrogel.

The AFM was used first to look at the initial topography of the undeformed hydrogel. The AFM hardware and software work together to output topography by utilizing the motor to keep track of how far the tip moves until it reaches its trigger force, and tracking that trigger force z-position as the surface z-position (Figure 2.7A). However, the inherent flaw in this method is that with a sample of varying stiffness, the tip will only indent shallowly into a stiff surface before reaching its trigger force, and deeply into a soft surface. Therefore, using this algorithm on a hypothetical surface that is perfectly smooth but varies in stiffness will show peaks at its stiff points and valleys at its soft points. For this experiment, a correction software (courtesy of Dr. Alex Fuhrmann) was able to circumvent this problem. Assuming that the sample is a viscoelastic solid, there should be two linear regions when the AFM force curve is transformed using a Hertzian model; one region where there is no change in deflection in relation to moving the motor in the z-direction before the tip contacts the surface, and another region where the deflection changes linearly with the change in z which occurs after the tip contacts the surface and is indenting in (Figure 2.7B). This software finds the slopes of these two linear regions and calculates where they should theoretically intersect to yield the surface z-position (Figure 2.7B). In this way, it can compensate for areas of higher or lower elastic modulus.

The results of these topography maps (Figure 2.8) show a relatively flat surface with a gradual slope over the wire. While the total height difference amount to ~5 μm, we postulated that it should not be a factor influencing cell behavior because of the scale of the gentle slope

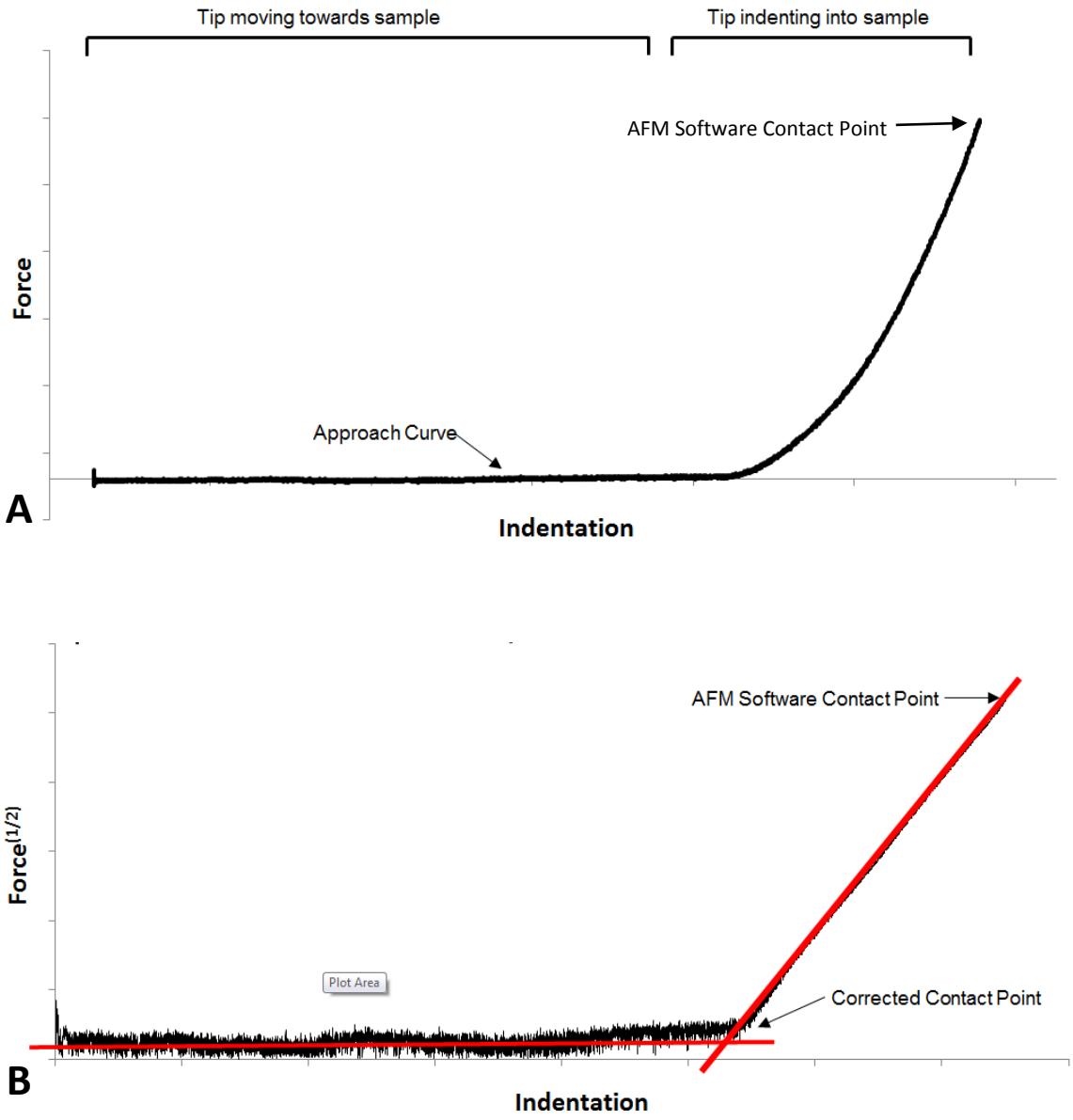

Figure 2.7. (A) AFM force curve and corresponding **(B)** Hertzian transformation highlighting the two linear regions and corrected contact point.

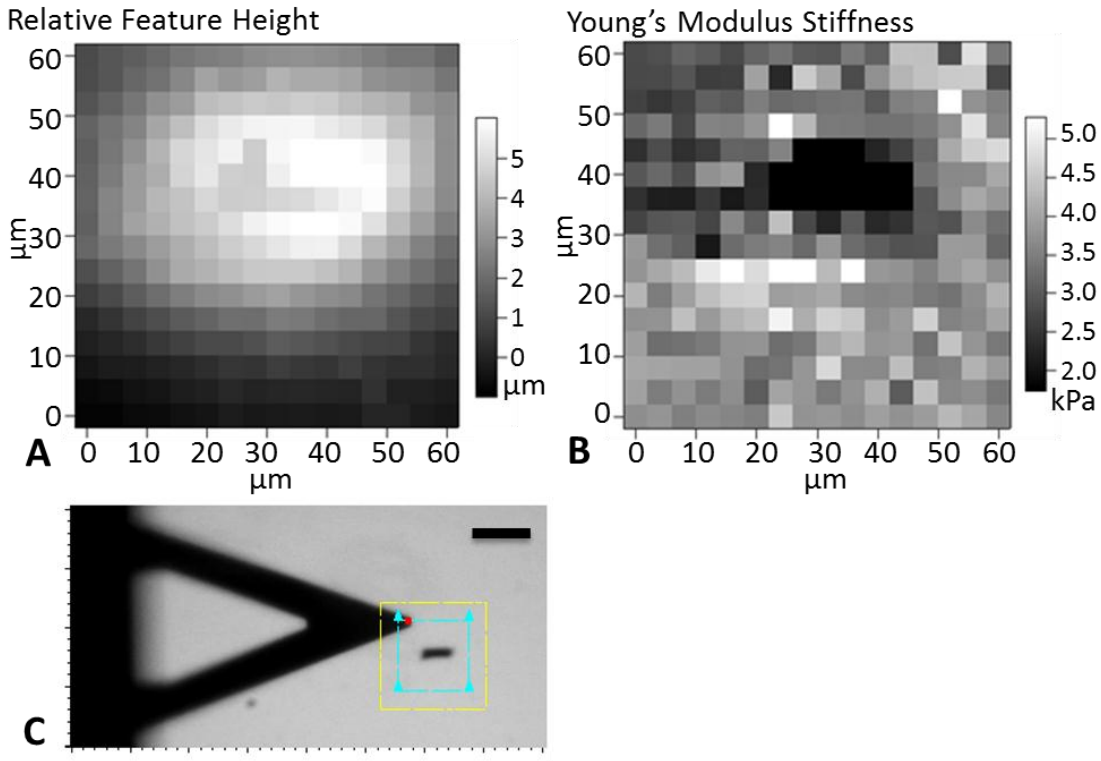

Figure 2.8. Effects of microwires on PA polymerization **(A)** Relative surface topography of hydrogel over a wire **(B)** PA stiffness decreases 2-fold over a microwire **(C)** Brightfield image of AFM scan. Yellow box outlines the maximum scan area; blue box outlines the scan area used (60µm x 50µm). Scale bar = 50 µm.

over the wire in comparison to the smaller wire-induced topography. However, to substantiate this hypothesis, we added an extra control in the cell experiments (Section 3.3.1)

The Young's modulus over a wire embedded in the hydrogel was also calculated from the slope of the second linear region of the Hertzian model. This relates the movement of the cantilever to the change in deflection, or the resistance of the material to indentation by the cantilever. The stiffness of the hydrogel was shown to increase to about 3 kPa over the microwire (Figure 2.8). The differences in topography and stiffness over the microwires were accounted for by adding an extra control hydrogel to the cell experiments. In addition to the static hydrogel control (with microwires but no magnetic actuation), a control of a static PA hydrogel with no wires was also included, but neither dataset shown, as both reflect previous data of uniform material [33].

2.2.4 Resistance to Viscoelastic Creep

The last parameter tested for this substrate was its tendency towards viscoelastic creep, or the plastic deformation of a sample under constant load at constant temperature over time [34]. Polymers, such as PA, are prone to exhibiting an initial strain when load is applied, but continuing to plastically deform over time. To test this, four sets of confocal stacks were acquired. At t=0 h, a set of images over a single wire with no magnetic actuation was acquired. Another set of images was taken immediately after in the presence of a magnetic field and the displacements were calculated (Figure 2.9A). The magnetic field was left in place for 24 h. A set of images was taken with the magnet in place; then the magnet was removed and a final set of images of the hydrogel in its undeformed state was acquired (Figure 2.9B). TFM analysis showed no significant difference in the displacement field between t=0 h and 24 h as compared to the initial undeformed state (t=0 h) (Figure 2.9C). Also, there was no significant change in

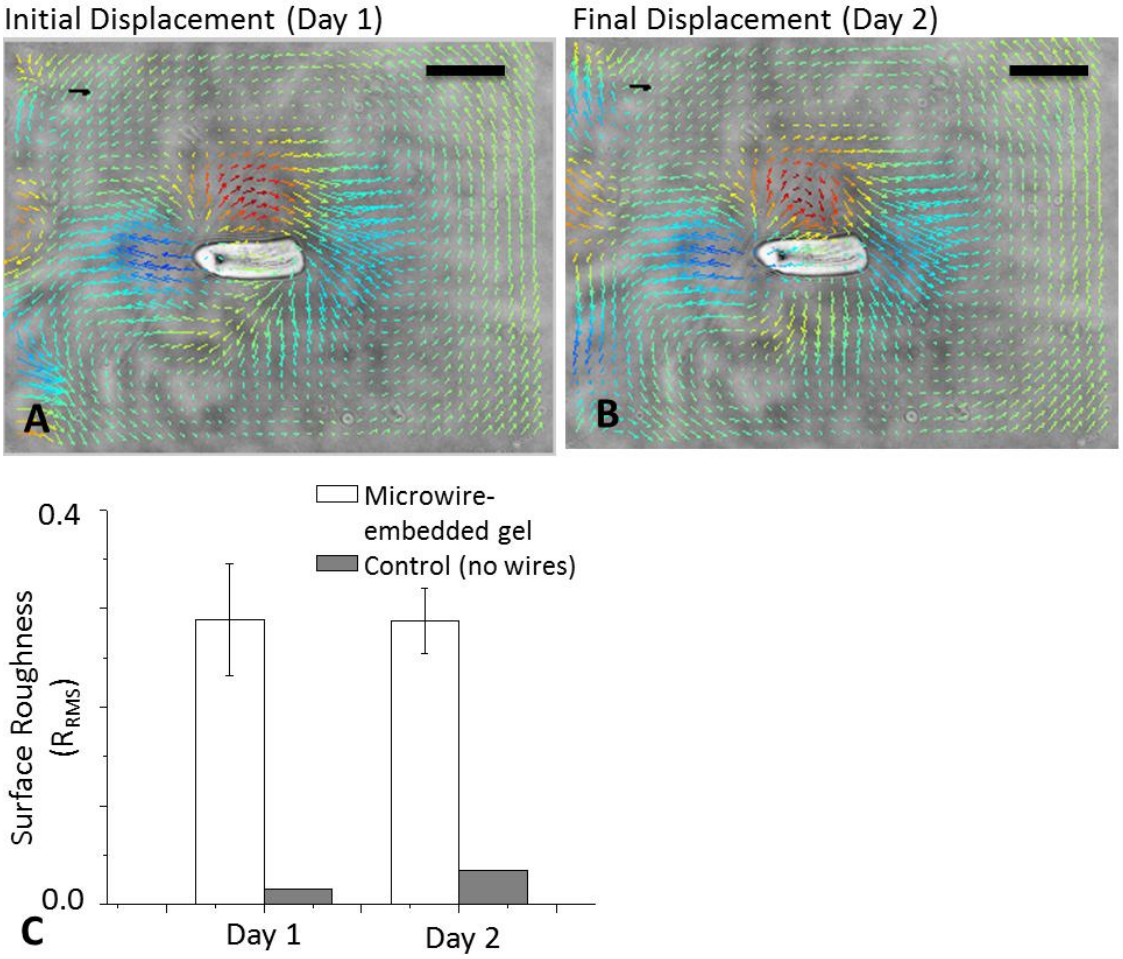

Figure 2.9. .Topographical features are resistant to viscoelastic creep. **(A)** Initial displacement field induced by a microwire in a magnetic field, t=0 h. Scale bar = 20 μm. **(B)** Displacement field after 20 h exposure to magnetic field; the displacement fields of (A) and (B) show no loss of features to viscoelastic creep. **(C)** TFM microscopy analysis shows no change in surface roughness over time (n=3).

displacement between the initial undeformed and final undeformed states, indicating that no plastic deformation occurs over the 24 h time period.

2.3 Conclusions

This substrate was able to generate microscale topographical changes in the surface of a soft hydrogel. by the magnetic deformation of microwires. The addition of microwires yielded small aberrations in the material properties of the hydrogel as characterized by AFM, leading to the addition of a wire-less control in the cell experiments. However, the features have been shown to remain robust over time, and should therefore be conducive to studying the effects of dynamic topography on cell culture.

Chapter III

Cellular Response to a Substrate with Dynamic Topography

3.1. Introduction

Once substrate synthesis had been optimized and the substrate itself fully characterized, it was important to understand cellular response in topography, i.e. from a smooth to a rough surface. We hypothesized that the cell's cytoskeleton should have some response to this topography change, and wanted to be able to track that response in real time. The second part of the cell work looked at the response over a longer time frame; in particular, how cells might react to a constantly changing topography. It aimed to compare the morphology of cell populations under static topography conditions (no magnetic actuation) to those that are under the stress of a continually changing topographical surface.

3.2 Methods

3.2.1 Cell Type

A7R5 rat smooth muscle cells were used to study the cellular response to the topographically dynamic substrate. These are large cells with easily identifiable cytoskeletal structures that have been previously used to look at the effect of substrate compliance (i.e. modulus) on spreading and cytoskeletal organization. These cells were cultured with Low Glucose DMEM (Gibco #18855) with 10% FBS, 2mM glutamine, and antibiotics/antimycotics, and 0.25% Trypsin-EDTA for passaging.

3.2.2. Transfection Protocol

To visualize the actin cytoskeleton, the cells were transfected with RFP-Actin, which, in addition to fluorescently illuminating the actin filaments, would slightly overexpress actin to improve cell attachment and viability on a soft substrate [35]. The plasmid, pTagRFP-N vector (Evrogen #FP142, courtesy of Dr. Shu Chien), was transformed into DH5α E.coli by heat shock at 42°C. 1 μL of 1μg/μL plasmid was added to 50 μL of E.coli culture. The transformed cells were plated onto LB/Kanamycin selection plates. Individual colonies were selected and grown in LB broth overnight. The culture was then purified using the stock solutions and protocol of the UltraClean 6-minute Mini Plasmid Preparation Kit (Mo Bio Laboratories, #12300-100). The plasmid concentration was then quantified by spectrophotometer at 260 nm. The plasmid was prepared in advance and stored at -20°C.

Lipofectamine 2000 was used to then transfect the mammalian cells. One day before the transfection, 40,000-50,000 cells were plated in each well of a 6-well plate and allowed to adhere and spread. On the day of the tranfection, culture media was removed and replaced with DMEM + 2% FBS (no antibiotics) to serum-starve cells. For each well, 4 μg of RFP-Actin were added to 250 μL of Opti-MEM Reduced serum media. In a separate tube, 5 μL of Lipofectamine 2000 were added to 250 μL of Opti-MEM and incubated for 5 min at room temperature. The RFP-Actin and Lipofectamine were then gently mixed and incubated for 20 min at room temperature. The low-serum media was then aspirated out of the wells, 1.5 mL of fresh low-serum media (DMEM + 2% FBS, no antibiotics) and 500 μL of complexes were added to each well. The complexes were then incubated with the cells at 37°C for 24 h. After 24 h (day 0 post-transfection), the transfection media was removed and replaced with normal culture media. On day 2 post-transfection, selection media (Low Glucose DMEM with 10% FBS, and streptomycin, penicillin, and neomycin) was added to select for plasmid-expressing cells. On days 3 and 4 post-transfection, the cells expressed the highest levels of RFP-Actin and were replated onto hydrogels for experiments.

3.2.3. Methods for Cellular Response to a Step-Function Topography Change

The cells used for this experiment were 3-4 days post-transfection to optimize RFP-Actin expression. Depending on the confluency (a function of the number of days post-transfection and the transfection survival rate), 1-2 wells of a 6-well plate were plated onto one 25 mm diameter wire-embedded hydrogel. The cells were allowed to adhere and spread for 4 h, then rinsed in fresh media to remove all non-adherent cells. The coverslip was then mounted onto a coverslip holder (ASI Imaging) with a LiveCell temperature control (Pathology Devices, Inc.), to maintain temperature, and a Nikon 60X high numerical aperture water immersion objective lens. It should be noted that because the LiveCell temperature control and the coverslip were manufactured by two different companies, they were not built to be interfaced. When used in this application, the LiveCell temperature control read out an incorrect temperature due to unanticipated heat transfer. This was likely due to the material properties of the coverslip holder, and the immersion lens acting as a heat sink to draw heat away from the coverslip. Using a thermocouple, it was determined that when the LiveCell temperature control was maximized (temperature control set at 70°C), the temperature at the coverslip was 32°C. While 32°C was not optimal for A7R5 viability, any temperature effects were compensated by adding cells to a simple two-layer PA hydrogel without microwires, as a control of cell behavior in that environment.

Once the coverslip had been mounted with the temperature control, images of transfected cells in the presence of wires were taken in both brightfield and with the Texas Red fluorescent filter at t=0 min. Subsequent fluorescent images were taken every 2 minutes for a total of 12 minutes. At t=14 min, the magnet was added, and a brightfield and fluorescent image was acquired for each cell. The fluorescent images were then acquired every two minutes until the contrast became minimal due to photobleaching.

3.2.4. Methods for Cellular Response to Dynamic Topography Modulation

To achieve continual magnetic oscillation, an incubator-safe magnetic actuator was designed to rotate the magnet at 1 Hz close to and then far away from the hydrogel as shown in Figure 3.1. When the magnet was in range to induce a topography change, it was in the same geometry as in the step function experiment. Like the step-function experiment, this experiment utilized cells 3-4 days post-transfection, plated at a density of 1-2 wells per hydrogel. Cells were seeded onto three hydrogels: two microwire-embedded hydrogels, and one control hydrogel without microwires. The cells were allowed to adhere and spread for 4 h, and then rinsed with media to remove all non-adherent cells. After 4 h, one microwire-embedded hydrogel was placed on the magnetic actuator to subject it to dynamic topography, while the two controls (one microwire-embedded and one control hydrogel) were cultured under static conditions. The cells were incubated under these conditions for 20-24 h, then fixed and mounted a slide. Fluorescent images (Texas Red filter) and brightfield images were acquired of cells with high RFP expression and their surrounding wires.

3.3. Results

3.3.1 Results of the Cellular Response to a Step-Function Topography Change

Consistent with previous results of A7R5's on a soft polyacrylamide hydrogel[35], most cells were not well-spread enough on the soft substrate to see well-defined individual actin filaments [35]; however, the area of the cell was usually well-defined, sometimes with a ring of brighter signal around the cell's perimeter (Figure 3.2). Cells selected for tracking also exhibited high RFP signal. The results for this experiment include following twelve cells with varying surface roughness between R_{RMS} = 0.175 μm and 0.522 μm and three control cells with no wires. The cells and corresponding roughnesses in ascending order were as follows:

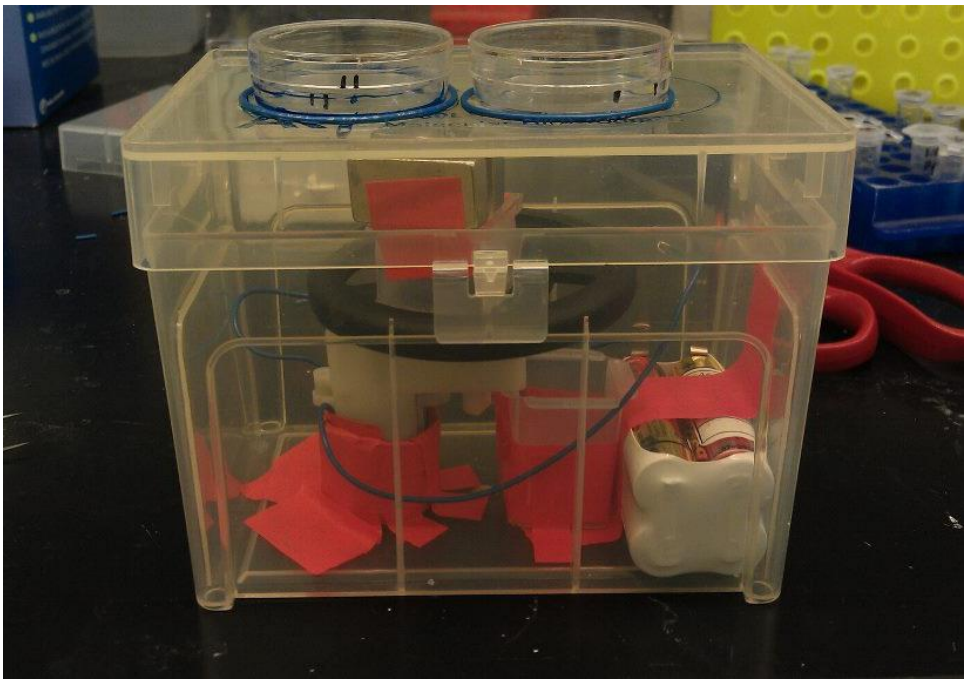

Figure 3.1. Magnetic actuator designed to reversibly induce a magnetic field to the coverslips. The battery-powered servo motor rotates the magnet alternatively between the two coverslip holders at ~60 RPM.

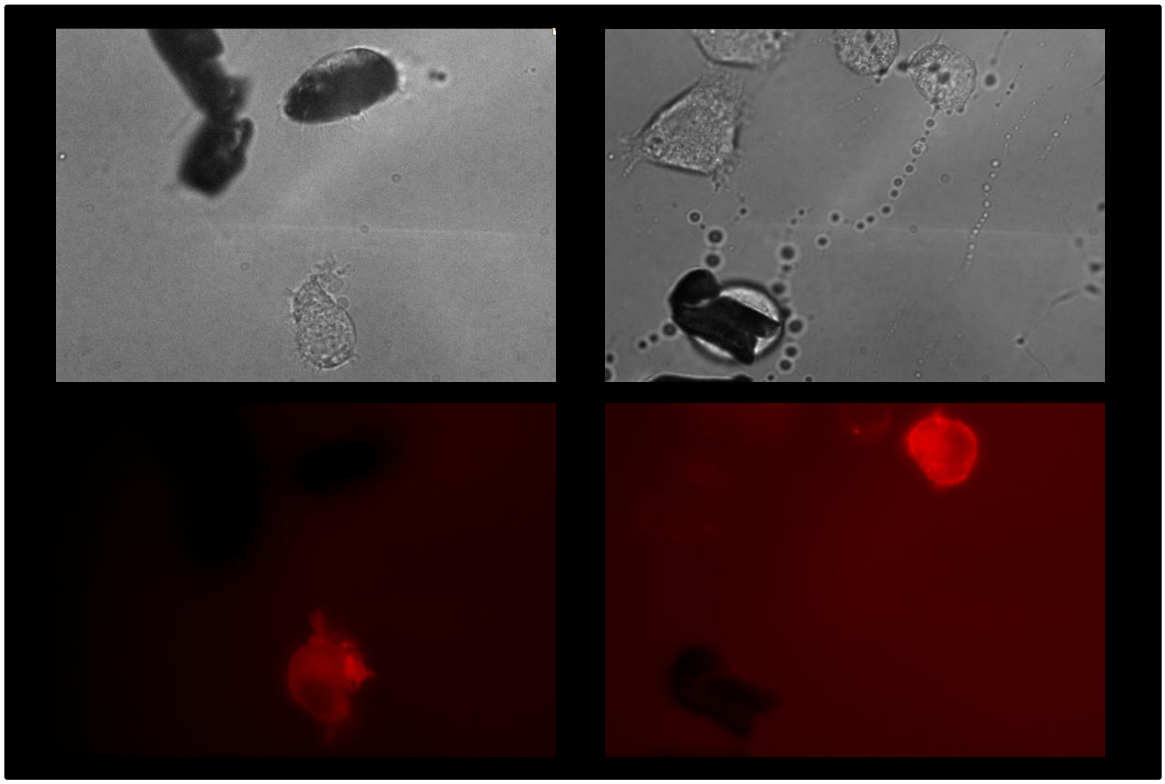

Figure 3.2. Representative images of cells with high RFP-Actin transfection levels and surrounding microwires in brightfield (top) and Texas Red (bottom).

Table 3.1. Summary of cells subjected to a step function topography change and their corresponding surface roughness values.

Experimental Group	Initial Cell Area in μm^2	Surface Roughness (R_{RMS}) in μm
Control	816.2	0.089
Control	733.7	0.089
Control	648.3	0.089
Wire	335.2	0.175
Wire	495.8	0.181
Wire	535.6	0.183
Wire	1255.5	0.183
Wire	421.2	0.186
Wire	300.9	0.239
Wire	898.5	0.268
Wire	939.5	0.345
Wire	443.1	0.363
Wire	713.1	0.429
Wire	493.6	0.514
Wire	375.8	0.522

Each image sequence was stacked to create a time lapse video of the cell's response to the topography change. Each image in the sequence was then thresholded individually to account for photobleaching effects. The primary endpoint for this experiment was to quantify the change in cell spread area, calculated by dividing the cell area at each time point by the initial cell area (at t=0 min).

$$Change\ in\ Cell\ Area = A_t/A_0 \quad (1)$$

To analyze these cells, the cells were binned into two categorizations. The data was first binned by initial cell spread area into a control group, a "small" cell group (A_0 = 301 μm^2 to 536 μm^2), and a "large" cell group (A_0 = 713 μm^2 to 1256 μm^2). The data was then binned by surface

roughness into a control group, a "low" surface roughness group (R_{RMS} = 0.175 to 0.186 μm), and a "high" surface roughness group (R_{RMS} = 0.238 to 0.522 μm). The changes in cell area were averaged over each group at each time point and plotted as a function of cell size (Figure 3.3A) and surface roughness (Figure 3.3B). It appears that a step function change in topography causes cells to decrease in area (Figure 3.4) but is not dependent on initial cell size. However, this decrease in cell spread area does seem to be dependent on surface roughness. While both roughness groups (R_{RMS} <200 nm, R_{RMS} >200 nm) were significantly different from the control group, it appears that a less rough surface (R_{RMS} < 200 nm) elicits a more gradual change in area, while a more rough surface induces a more immediate change.

3.3.2 Results of the Cellular Response to Dynamic Topography Modulation

To analyze the cells, a perimeter was hand-drawn around the brightfield images and thresholded. The brightfield images were used instead of Texas Red because some of the fluorescent actin did not extend into the lamellopodia. Because this experiment compares populations of cells, instead of a single cell to itself over time, it was important to accurately determine the area of the cell. In addition to the cell area, the length of the major and minor axis of the cell, and the cell angle, were also calculated. The primary endpoints of this experiment were cell spread area and spindle factor. Cell spread area was calculated in μm^2 from the thresholded image of the cell. The spindle factor is a metric used by Engler and co-workers, [28] and others, which is defined by:

$$Spindle\ Factor = [major\ axis]/[minor\ axis] \quad (2)$$

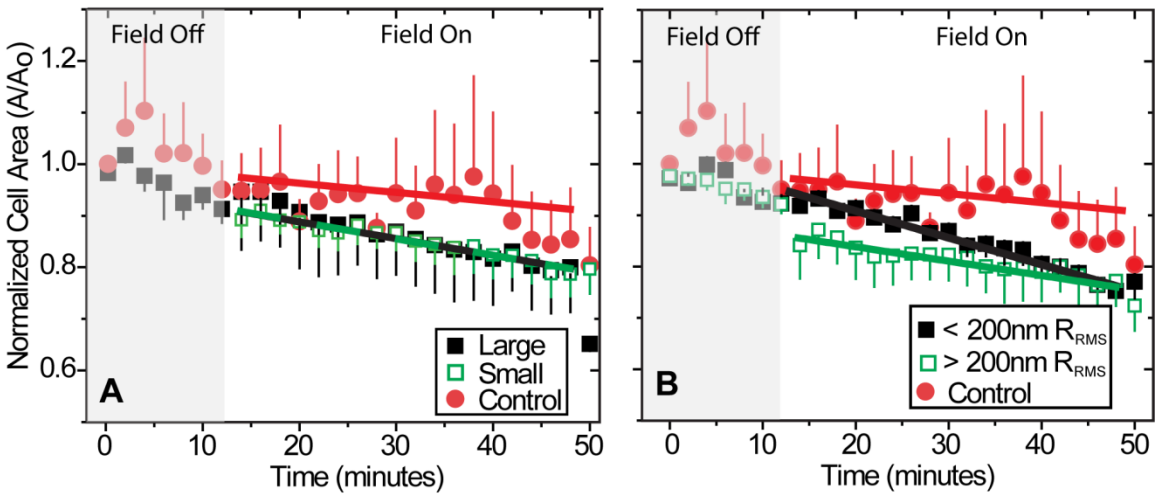

Figure 3.3. Change in cell area (A/A_0) as a function of time. Cells were binned **(A)** by size and **(B)** by surface roughness. Analysis of covariance (ANCOVA) between two groups indicates that for (A), only the difference between the control and large cells was statistically significant ($p<0.001$) and for (B), the difference between all of the groups was statistically significant ($p<0.005$). Error bar = SEM.

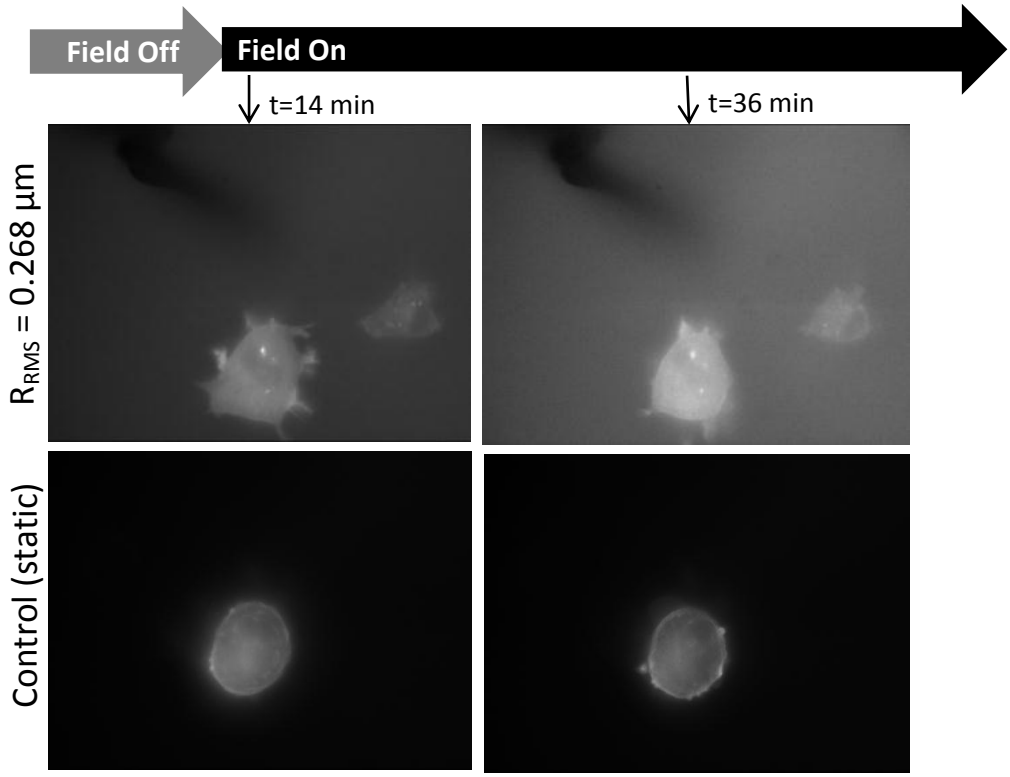

Figure 3.4. Cell area decrease in response to magnetic actuation. A cell introduced to a step function change in topography (R_{RMS} = 0.268µm) (top) and a static (control) cell (bottom) at t = 14 min (left), immediately after the magnetic field was activated, and at t = 36 min (right). The cell on the dynamic surface decreases in area significantly more rapidly than the control cell.

This metric is such that a perfectly circular cell would have a spindle factor of 1, and a polarized cell would have a spindle factor greater than 1.

Before looking at the effect of the dynamic topography on the cell populations, it was imperative to verify our earlier hypothesis, that the microwires would have no effect on the cells in terms of any changes in stiffness and undeformed topography. This was done by comparing the control gel (no microwires) to the static gel (microwires but no magnetic actuation). Figure 3.5A and B show that based on the spindle factor and cell spread area, there is no significant difference between the cells on the control and static gels. Calculation of the orientation correlation factor (OCF) also confirmed that the cells were not affected by the wire stiffness (Figure 3.5C). The OCF is defined as:

$$OCF = \frac{1}{2}[\cos(2\theta) + 1] \tag{3}$$

where Θ is defined as the angle difference between each cell and each wire. An average OCF of 0 would indicate that the cells were oriented in the same direction as the wires. An average OCF of 1 would indicate that the cells were oriented in the opposite (180°) direction as the wires. An average OCF of 0.5 would indicate no correlation between the cell and wire orientations. The OCF was calculated for both the static and dynamic coverslips (it is not applicable for the control group, since there are no wires to orient with). Based on Figure 3.5, it can be assumed that the presence of wires in the gel, and any effect that they might have on cell morphology, is negligible.

Once the wires were established to have no effect on cell morphology, the analysis focused on the effect of dynamically oscillating surface topography on cell morphology. In Figure 3.6, the cell spread area for each cell was plotted in relation to its surface roughness,

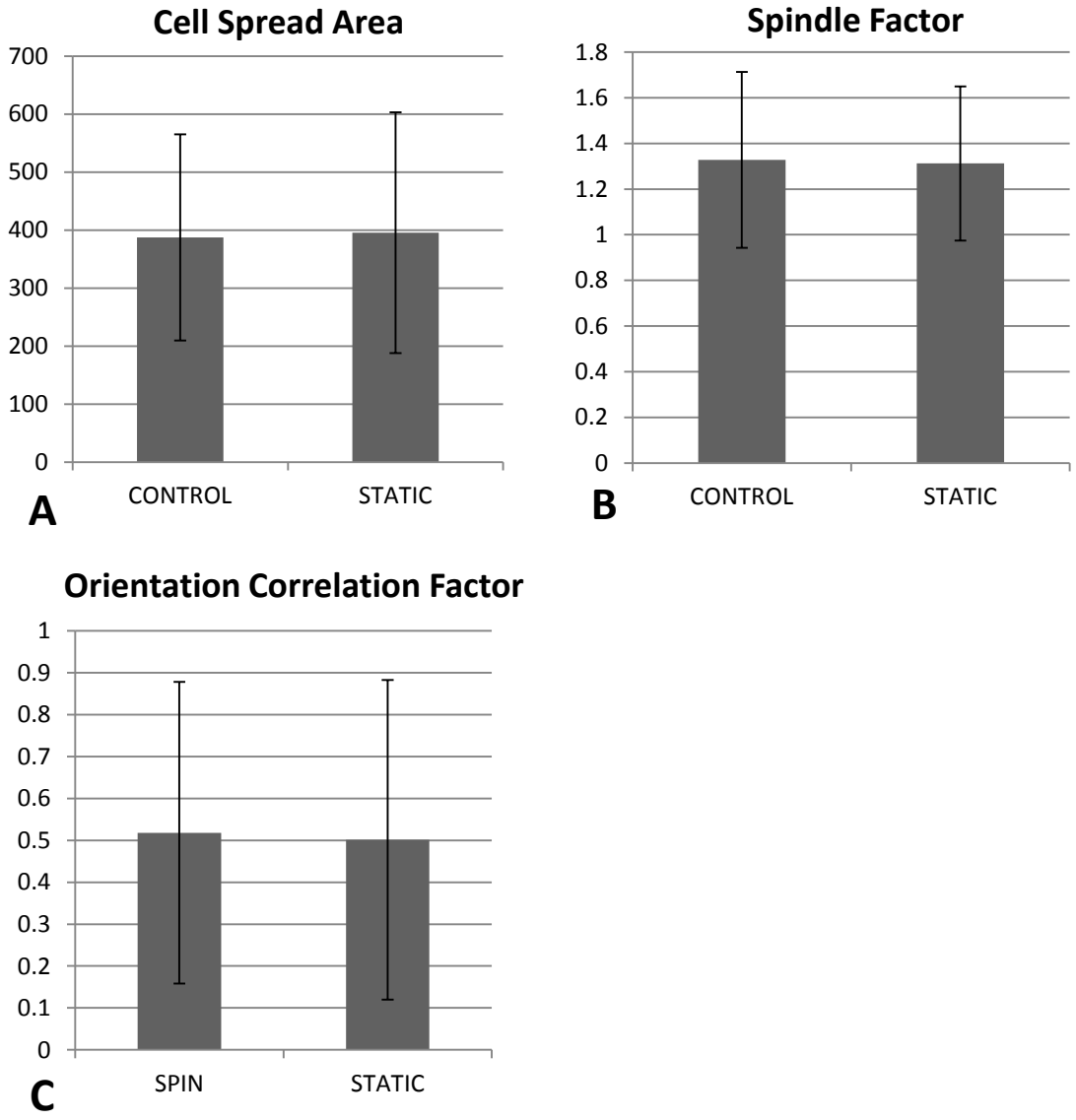

Figure 3.5. No significant difference between cell spread area (p=0.934) and spindle factor (p=0.771) indicate no effect of embedded microwires on cell morphology. OCF of both the static and dynamic coverslips show that the cells do not orient preferentially in the axis of the wires (p=0.785).

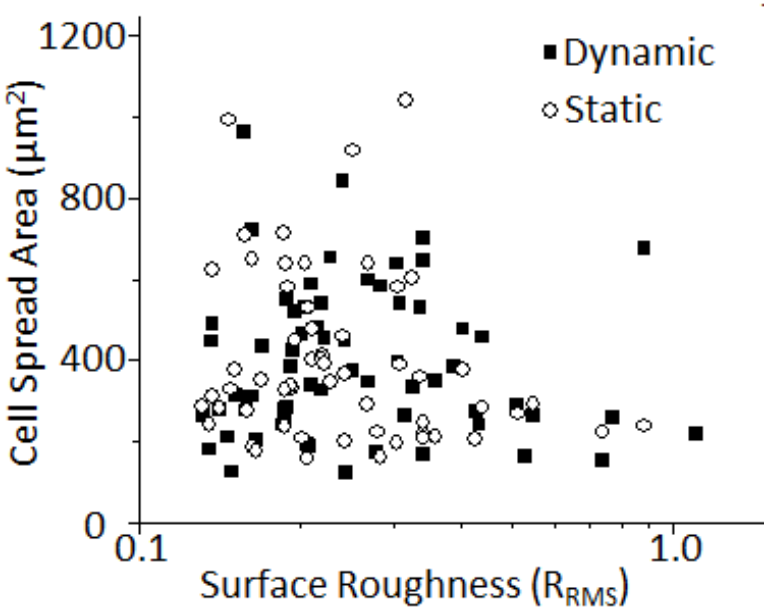

Figure 3.6. Relationship between surface roughness and cell spread area for dynamic and static cell populations.

calculated from the thresholded wire area using the correlation function in Figure 2.4. The correlation between surface roughness and both cell spread area and spindle factor appears to be relatively low. A possible explanation is that within the 24 h time period, the cells have time to internally rearrange their cytoskeleton and position to best cope with the changing topography. If the cells have time to figure out the patterns of how the topography is changing, it could arrange itself to be least affected by the topographical effects and therefore mitigate any global changes that would be observed in either spread area or spindle factor.

Chapter IV

Conclusions

Through this project, a topographically unique cell culture substrate was introduced. This substrate was distinctive because of its ability to reversibly induce topography changes despite some limitations in creating modest lateral strains. This preliminary cell experiments, however, primarily demonstrated that cells appear to respond at short time intervals to a change in topography, but can remodel themselves to adjust to their environment over time. This response seems to be dependent on how much the cell is initially spread. If the cell is initially large and well-spread, it can detect these topographical changes more acutely and thus react more drastically. However, over a longer time frame, for example continuous modulation over 24h, it appears that cells can position themselves in terms of their geometry and position to mitigate the effects of the changing topography. Therefore, there appears to be no significant difference between cells that have been subjected to the prolonged dynamic topography and those that have not.

Beyond what this project has explored, there are potentially many other ways to modulate this platform so that it can be used for slightly different applications. For example, the potential to modulate the substrate stiffness could elucidate the interplay between the role of stiffness and topography in general cell behavior, and more specifically, stem cell differentiation. Also, changing the type or orientation of the magnetic particles could yield different topographies as well as induce different order within the matrix, e.g. nematic ordering of cells; aligning the particles with a magnetic field pre-polymerization could yield an organized, as opposed to random topography. By introducing the controllable variables of substrate stiffness and time-

dependent topography, this thesis is able to broaden the study of how microenvironment topography affects cell behavior, and will hopefully lead to a better understanding of the factors that are involved with microscale cell niches.

REFERENCES

1. Discher, D.E., D.J. Mooney, and P.W. Zandstra, *Growth factors, matrices, and forces combine and control stem cells.* Science, 2009. **324**(5935): p. 1673-7.

2. Ding, S. and P.G. Schultz, *A role for chemistry in stem cell biology.* Nat Biotechnol, 2004. **22**(7): p. 833-40.

3. Reilly, G.C. and A.J. Engler, *Intrinsic extracellular matrix properties regulate stem cell differentiation.* J Biomech, 2010. **43**(1): p. 55-62.

4. Prabhakaran, M.P., J.R. Venugopal, and S. Ramakrishna, *Mesenchymal stem cell differentiation to neuronal cells on electrospun nanofibrous substrates for nerve tissue engineering.* Biomaterials, 2009. **30**(28): p. 4996-5003.

5. Martino, S., F. D'Angelo, I. Armentano, R. Tiribuzi, M. Pennacchi, M. Dottori, S. Mattioli, A. Caraffa, G.G. Cerulli, J.M. Kenny, and A. Orlacchio, *Hydrogenated amorphous carbon nanopatterned film designs drive human bone marrow mesenchymal stem cell cytoskeleton architecture.* Tissue Eng Part A, 2009. **15**(10): p. 3139-49.

6. Karuri, N.W., S. Liliensiek, A.I. Teixeira, G. Abrams, S. Campbell, P.F. Nealey, and C.J. Murphy, *Biological length scale topography enhances cell-substratum adhesion of human corneal epithelial cells.* J Cell Sci, 2004. **117**(Pt 15): p. 3153-64.

7. Ranucci, C.S. and P.V. Moghe, *Substrate microtopography can enhance cell adhesive and migratory responsiveness to matrix ligand density.* J Biomed Mater Res, 2001. **54**(2): p. 149-61.

8. Kaiser, J.P., A. Reinmann, and A. Bruinink, *The effect of topographic characteristics on cell migration velocity.* Biomaterials, 2006. **27**(30): p. 5230-41.

9. Kim, D.H., C.H. Seo, K. Han, K.W. Kwon, A. Levchenko, and K.Y. Suh, *Guided Cell Migration on Microtextured Substrates with Variable Local Density and Anisotropy.* Adv Funct Mater, 2009. **19**(10): p. 1579-1586.

10. Teixeira, A.I., G.A. McKie, J.D. Foley, P.J. Bertics, P.F. Nealey, and C.J. Murphy, *The effect of environmental factors on the response of human corneal epithelial cells to nanoscale substrate topography.* Biomaterials, 2006. **27**(21): p. 3945-54.

11. Liliensiek, S.J., S. Campbell, P.F. Nealey, and C.J. Murphy, *The scale of substratum topographic features modulates proliferation of corneal epithelial cells and corneal fibroblasts.* J Biomed Mater Res A, 2006. **79**(1): p. 185-92.

12. Rowland, T.J., L.M. Miller, A.J. Blaschke, E.L. Doss, A.J. Bonham, S.T. Hikita, L.V. Johnson, and D.O. Clegg, *Roles of integrins in human induced pluripotent stem cell growth on Matrigel and vitronectin.* Stem Cells Dev, 2010. **19**(8): p. 1231-40.

13. Wan, Y., Y. Wang, Z. Liu, X. Qu, B. Han, J. Bei, and S. Wang, *Adhesion and proliferation of OCT-1 osteoblast-like cells on micro- and nano-scale topography structured poly(L-lactide).* Biomaterials, 2005. **26**(21): p. 4453-9.

14. McNamara, L.E., R.J. McMurray, M.J. Biggs, F. Kantawong, R.O. Oreffo, and M.J. Dalby, *Nanotopographical control of stem cell differentiation.* J Tissue Eng, 2010. **2010**: p. 120623.

15. Jin, G., M.P. Prabhakaran, and S. Ramakrishna, *Stem cell differentiation to epidermal lineages on electrospun nanofibrous substrates for skin tissue engineering.* Acta Biomater, 2011. **7**(8): p. 3113-22.

16. Li, W.J., R. Tuli, C. Okafor, A. Derfoul, K.G. Danielson, D.J. Hall, and R.S. Tuan, *A three-dimensional nanofibrous scaffold for cartilage tissue engineering using human mesenchymal stem cells.* Biomaterials, 2005. **26**(6): p. 599-609.

17. Li, W.J., R. Tuli, X. Huang, P. Laquerriere, and R.S. Tuan, *Multilineage differentiation of human mesenchymal stem cells in a three-dimensional nanofibrous scaffold.* Biomaterials, 2005. **26**(25): p. 5158-66.

18. Choi, Y.S., *Engineered ECM Microenvironments and their Regulation of Stem Cells*, 2012.

19. Martinez, E., E. Engel, J.A. Planell, and J. Samitier, *Effects of artificial micro- and nano-structured surfaces on cell behaviour.* Ann Anat, 2009. **191**(1): p. 126-35.

20. Curtis, A. and C. Wilkinson, *Topographical control of cells.* Biomaterials, 1997. **18**(24): p. 1573-83.

21. Dalby, M.J., N. Gadegaard, R. Tare, A. Andar, M.O. Riehle, P. Herzyk, C.D. Wilkinson, and R.O. Oreffo, *The control of human mesenchymal cell differentiation using nanoscale symmetry and disorder.* Nat Mater, 2007. **6**(12): p. 997-1003.

22. Chew, S.Y. and W.C. Low, *Scaffold-based approach to direct stem cell neural and cardiovascular differentiation: an analysis of physical and biochemical effects.* J Biomed Mater Res A, 2011. **97**(3): p. 355-74.

23. Dulgar-Tulloch, A.J., R. Bizios, and R.W. Siegel, *Human mesenchymal stem cell adhesion and proliferation in response to ceramic chemistry and nanoscale topography.* J Biomed Mater Res A, 2009. **90**(2): p. 586-94.

24. Khor, H.L., Y. Kuan, H. Kukula, K. Tamada, W. Knoll, M. Moeller, and D.W. Hutmacher, *Response of cells on surface-induced nanopatterns: fibroblasts and mesenchymal progenitor cells.* Biomacromolecules, 2007. **8**(5): p. 1530-40.

25. Maclaine, S.E., N. Gadhari, R. Pugin, R.M. Meek, M. Liley, and M.J. Dalby, *Optimizing the osteogenicity of nanotopography using block co-polymer phase separation fabrication techniques.* J Orthop Res, 2012.

26. Dalby, M.J., M.O. Riehle, H.J. Johnstone, S. Affrossman, and A.S. Curtis, *Nonadhesive nanotopography: fibroblast response to poly(n-butyl methacrylate)-poly(styrene) demixed surface features.* J Biomed Mater Res A, 2003. **67**(3): p. 1025-32.

27. Oh, S., K.S. Brammer, Y.S. Li, D. Teng, A.J. Engler, S. Chien, and S. Jin, *Stem cell fate dictated solely by altered nanotube dimension.* Proc Natl Acad Sci U S A, 2009. **106**(7): p. 2130-5.

28. Engler, A.J., S. Sen, H.L. Sweeney, and D.E. Discher, *Matrix elasticity directs stem cell lineage specification.* Cell, 2006. **126**(4): p. 677-89.

29. Tse, J.R. and A.J. Engler, *Preparation of hydrogel substrates with tunable mechanical properties.* Curr Protoc Cell Biol, 2010. **Chapter 10**: p. Unit 10 16.

30. Sniadecki, N.J., A. Anguelouch, M.T. Yang, C.M. Lamb, Z. Liu, S.B. Kirschner, Y. Liu, D.H. Reich, and C.S. Chen, *Magnetic microposts as an approach to apply forces to living cells.* Proc Natl Acad Sci U S A, 2007. **104**(37): p. 14553-8.

31. Boudou, T., J. Ohayon, C. Picart, and P. Tracqui, *An extended relationship for the characterization of Young's modulus and Poisson's ratio of tunable polyacrylamide gels.* Biorheology, 2006. **43**(6): p. 721-8.

32. Radmacher, M., R.W. Tillamnn, M. Fritz, and H.E. Gaub, *From molecules to cells: imaging soft samples with the atomic force microscope.* Science, 1992. **257**(5078): p. 1900-5.

33. Flores-Merino, M.V., S. Chirasatitsin, C. Lopresti, G.C. Reilly, G. Battaglia, and A.J. Engler, *Nanoscopic mechanical anisotropy in hydrogel surfaces.* Soft Matter, 2010. **6**(18): p. 4466-4470.

34. Christman, K.L., *Lecture, Principles of Biomaterials Design*, in *BENG 186A*2009.

35. Engler, A.J., Bacakova, L., Newman, C., Hategan, A., Griffin, M., Discher, D.E., *Substrate Compliance versus Ligand Density in Cell on Gel Responses.* Biophys J, 2004. **86**: p. 617-628.